Response Function Estimation for In-Core Bf3 and ^{3}He Neutron Detectors Using MCNPX - Case Study of Opal Reactor

B. Oryema[1*], M. A. M. Nader[2], and S. A. E. Agamy[3]

[1]Department of Physics, Busitema University, P.O Box 236 Tororo, Uganda
[2]Egyptian Atomic Energy Authority, ETRR-2, Cairo, Egypt
[3]Department of Nuclear & Radiation Engineering, Alexandria University, Egypt

ABSTRACT

In this study, the response functions of BF_3 and ^{3}He neutron proportional counters were estimated using the general purpose Monte Carlo simulation code, MCNPX. Open Pool Australian Light-water (OPAL) research reactor core was simulated and used as case study, and parameters such as the effects of increasing tube pressure and tube diameter on response functions were also investigated. It was observed that the pulse height spectrum for BF_3 counter had two sharp peaks at 2.31 MeV and 2.79 MeV, whereas that of ^{3}He counter was seen to have only one sharp peak at 0.76 MeV. The response matrices were observed to increase with increasing tube pressure and tube diameter. Also increasing the tube pressure and tube diameters were seen to increase pulse heights, and reduce the wall-effect phenomenon.

Keywords: Response functions, Pulse heights, Thermal neutron detectors, MCNPX simulation

INTRODUCTION

In a nuclear reactor, adequate instrumentation is required to ensure correct and safe operation of the reactor by providing information on system performance [1]. Several types of measurements are usually made in nuclear reactors; these include among others measurement of neutron flux, temperature, coolant flow, liquid level, strain in reactor vessel, pressure, and measurements of the quantity of any radioactive material in the coolant [1,2]. Neutron flux monitoring and measurement is important because it gives an indication of the reactor power. Monitoring flux from start-up range to power range also helps to control the fission chain reactions occurring within the reactor fuel meat [3]. Different types of neutron detectors have long been adapted for nuclear instrumentation, among them are: self-powered neutron detectors, proton recoil counters, activation foil detectors and specialized gas-filled detectors such as fission counters, ^{3}He counters, BF_3 counters and boron-lined counters [4].

The BF_3 and ^{3}He gas-filled proportional counters are known for having immensely higher thermal neutron absorption cross sections and sensitivities, which make them some of the best candidates for thermal neutron flux measurements in a nuclear reactor. In this study, the general purpose Monte Carlo code, MCNPX [5,6], was used to simulate response functions of cylindrical ^{3}He and BF_3 proportional counters to thermal neutrons in Open Pool Australian Light-water (OPAL) research reactor. As it's well documented in literatures [3,7], ^{3}He gas is the most suitable neutron sensitive gas used for making detectors because of its favorable properties such as high neutron absorption cross-section (5330 barns), chemical inertness and good behavior in proportional counters at high pressures [8]. ^{3}He detector is based on a thermal neutron absorption reaction with the emission of proton and triton which are easily detectable charged particles inside the detector sensitive volume as they ionize the fill-gas [7,8]. However, the supply of ^{3}He has become limited and the present demand level can no longer be sustained. One of the best alternative technologies for replacing ^{3}He is the BF_3 gas-filled proportional counter [1,9].

BF_3 detectors are based on thermal neutron absorption by ^{10}B, with the release of α-particle and ^{7}Li recoil nucleus which deposit their kinetic energies inside the fill-gas, causing ionization. Much as this detector type has a lower

neutron absorption cross-section compared to ^{3}He based detector, BF_3 gas is easily available and has a better gamma discrimination capability than the ^{3}He counter. This is because there are higher levels of gamma energy deposition in BF_3 which allows better gamma pulse discrimination than in the ^{3}He [1,9]. In principle, BF_3 counters can be operated in a gamma field up to 100-200 R/h while ^{3}He can be operated in gamma fluxes of up only 1R/h [1,2,10]. Because of their high thermal neutron cross sections, ^{3}He and BF_3 counters can be best suited for neutron flux monitoring at the start-up and intermediated power ranges [7,9,10].

MATERIALS AND METHODS

Simulated neutron source

The Open Pool Australian Light-water (OPAL) reactor core was modeled in this study as the source of neutron. The reactor is a 20 MW thermal, multi-purpose, pool-type designed to deliver neutron beams across a broad range of energies [11]. Figure 1 illustrates the arrangement of fuel elements inside OPAL reactor core.

The reactor core has 16 low enriched uranium (LEU) fuel elements in a 4 × 4 grid array surrounded by zinc alloy chimney and no irradiation facilities within the core itself. Reactivity control is provided by five hafnium control rods. Each fuel element fed in the OPAL reactor consists of 21 aluminum-cladded fuel plates separated from each other by a 0.245 cm coolant channel. The active zone of fuel plate dimensions is; 61.5 cm length, 6.5 cm width and 0.061 cm thickness. The fuel plate meat is made of fine and homogeneous dispersion of U_3Si_2 particles with an enrichment of 19.75% in weight of ^{235}U, in a continuous matrix of pure commercially aluminum [11] (Figure 2).

Figure 2 shows typical configuration of fuel plates in a fuel element. The plates are supported by two aluminum guide plates and spacing between them filled with light water. The grid plates and fuel cladding materials are made of Al-6061. The cladding thickness is 0.037 cm. The basic geometric unit in the x-y core array is a square (8.15 × 8.15 cm^2) that houses a 8.05 × 8.05 cm^2 fuel element. Table 1 summarizes information about the main specifications of the simulated OPAL reactor core.
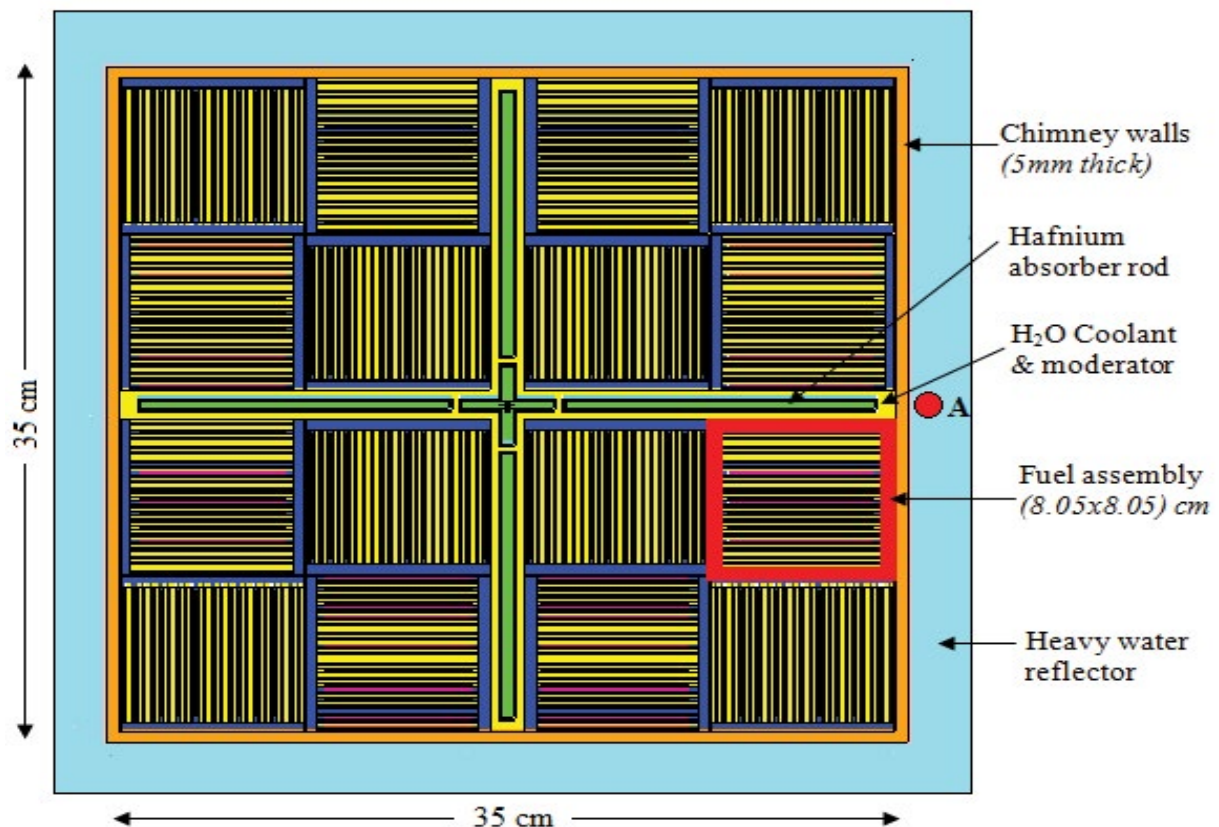

Figure 1: X-Y scheme of the simulated reactor core. A is the detector position
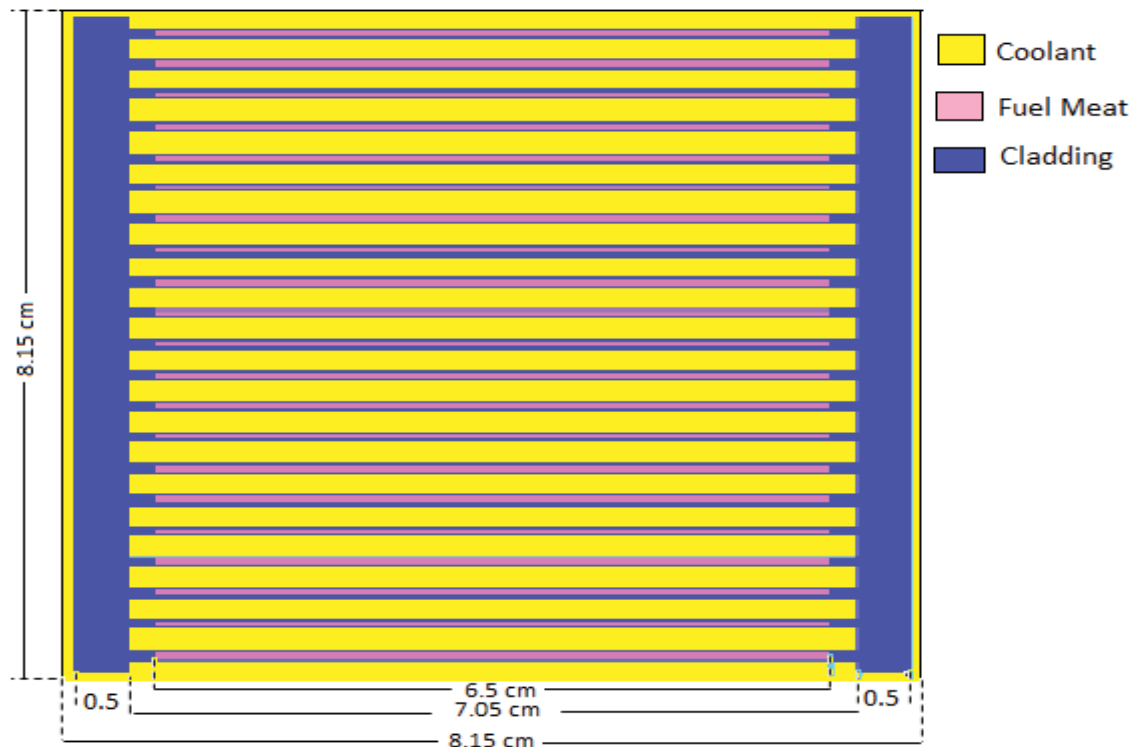
Figure 2: X-Y scheme of the simulated fuel element

Table 1: Main specifications of the simulated reactor core

Parameters	Dimension/composition
Core dimensions	35 cm × 35 cm × 61.5 cm
Coolant and moderator	Light water
Reflector	Heavy water
Number of control rods	5
Control rod material	Hafnium
Number of fuel elements	16
Number of fuel plates per element	21
Fuel plate thickness	0.135 cm
Fuel plate width	7.05 cm
Side plate thickness	0.5 cm
Side plate width	8.05 cm
Al density	2.7 g/cm^3
Meat thickness	0.061 cm
Meat width	6.5 cm
Meat length	61.5 cm
Meat cladding material	Al-6061 alloy
Meat cladding thickness	0.037 cm
Fuel meat density	6.5 g/cm^3
Fuel meat materials	U_3Si_2-Al matrix
Weight fraction --- ^{234}U (%)	0.105866
Weight fraction --- ^{235}U (%)	14.5645
Weight fraction --- ^{236}U (%)	0.058214
Weight fraction --- ^{238}U (%)	58.7951
Weight fraction --- Si (%)	5.78942
Weight fraction --- Al (%)	20.6923

Simulated neutron detectors

The detectors modelled for this thesis were the BF_3 and ^{3}He proportional counters manufactured by LND, INC; USA. The detector configurations were modeled in arbitrary 3-dimensional configuration and positioned at position A as shown in Figure 1. Table 2 shows the main specifications of the simulated detectors.

Table 2: Main specifications of the simulated LND detectors

Specifications	BF$_3$ Counter	^{3}He Counter
Model	2029	2523
Fill gas	BF$_3$	^{3}He
Gas pressure	400 torr~0.5 atm	7600 torr~10 atm
Cathode material	St. steel	St. steel
Maximum length (cm)	39.065	39.497
Effective length (cm)	31.115	30.48
Maximum diameter (cm)	2.54	2.54
Effective diameter (cm)	2.438	2.438
Effective volume (cm^3)	145.23	142.26

Procedures for calculating response functions

In this study, the response functions of ^{3}He and BF$_3$ counters were calculated using two different approaches. The first approach is based on simulating the number of absorption reactions ^{3}He (n,p) ^{3}H and ^{10}B (n,a) ^{7}Li inside ^{3}He and BF$_3$ counters respectively [12]. By using this approach, MCNP calculates the response, *R(E)*, of each detector assembly as the number of absorption reaction per unit neutron fluence (in unit of cm^2). This number is obtained from the track length estimate (F4 tally) and the associated FM card by using the appropriate multiplication factors as shown in Equation 1 [13];

$$R(E) = C \int \sigma(v, \gamma) \varphi(E) dE \qquad\qquad (1)$$

where

$\varphi(E)$ is the energy-dependent particle fluence (particle/cm^2) as estimated by the F4 tally, $\sigma(n, \gamma)$ (10^{-24} cm^2) is the cross-section tabulated values for ^{10}B (n,α) ^{7}Li or ^{3}He (n,p) ^{3}H absorption reactions. The constant *C* is any arbitrary scalar quantity that can be used for normalization. For *C*>0, MCNP multiplies the tally by *C*; while for *C*<0, it multiplies the tally by |*C*| and by atom density in the tally cell [13].

The second approach for calculating response functions was a more detailed model that tracked the emitted charged particles, and the corresponding pulse height energy deposition within the detector. MCNPX has the capability of tracking and scoring the pulse height energy depositions of charged particles by using F8 tally, and the associated physics models and special tally treatment (FT) cards [6]. For the case of ^{3}He counter, the emitted proton and triton were tracked and their energy depositions scored, whereas for the BF$_3$, the emitted alpha particles and lithium ions were tracked. The ISABEL and Bertin models were used in this simulation by activating them from the 3rd entry on the LCA card. Also, the NCIA which is the 7th entry on the PHYS:N card was turned on to help create charged secondary particles with correct energy and correlated angular distributions. FT card with PHL option was also included in this model. PHL option allows the F8 tally to be based on energy/light deposition in one or two other regions as specified via one or two F6 tallies, in which the F6 tallies convert energy deposition to equivalent light.

RESULTS AND DISCUSSION

Response functions in terms of number of absorption reactions

Figure 3 shows the estimated energy-dependent response functions of the BF$_3$ and ^{3}He counters in terms of the simulated numbers of ^{10}B (n,α) ^{7}Li and ^{3}He (n,p) ^{3}H absorption reactions in the two detectors, respectively. The calculations were performed for neutrons with energy in the range 0.01-0.1 eV.

It's clearly seen from Figure 3 that ^{3}He counter recorded higher response than BF$_3$ counter. BF$_3$ counter registered maximum response of about 85 cm^2/eV/fission neutrons at thermal neutron energy of about 0.015 eV. On the other hand, ^{3}He counter registered a much higher maximum response of about 240 cm^2/eV/fission neutrons at thermal neutron energy of about 0.025 eV. The high response observed for ^{3}He counter could be due to the fact that ^{3}He (n,p) ^{3}H reaction has a significantly higher thermal neutron cross section (5330 barns) as compared to ^{10}B (n,α) ^{7}Li reaction (3840 barns) in BF$_3$ counter [10]. Thus, ^{3}He counters are more sensitive to thermal neutrons than boron detectors.

The main disadvantage of using number of absorption reactions as the basis for response functions estimation is that it does not give information about energy depositions by charged particles generated from the reactions. When the generated charged particles recoil at high speed, they create primary ion pairs and thus, ionize the gas inside the
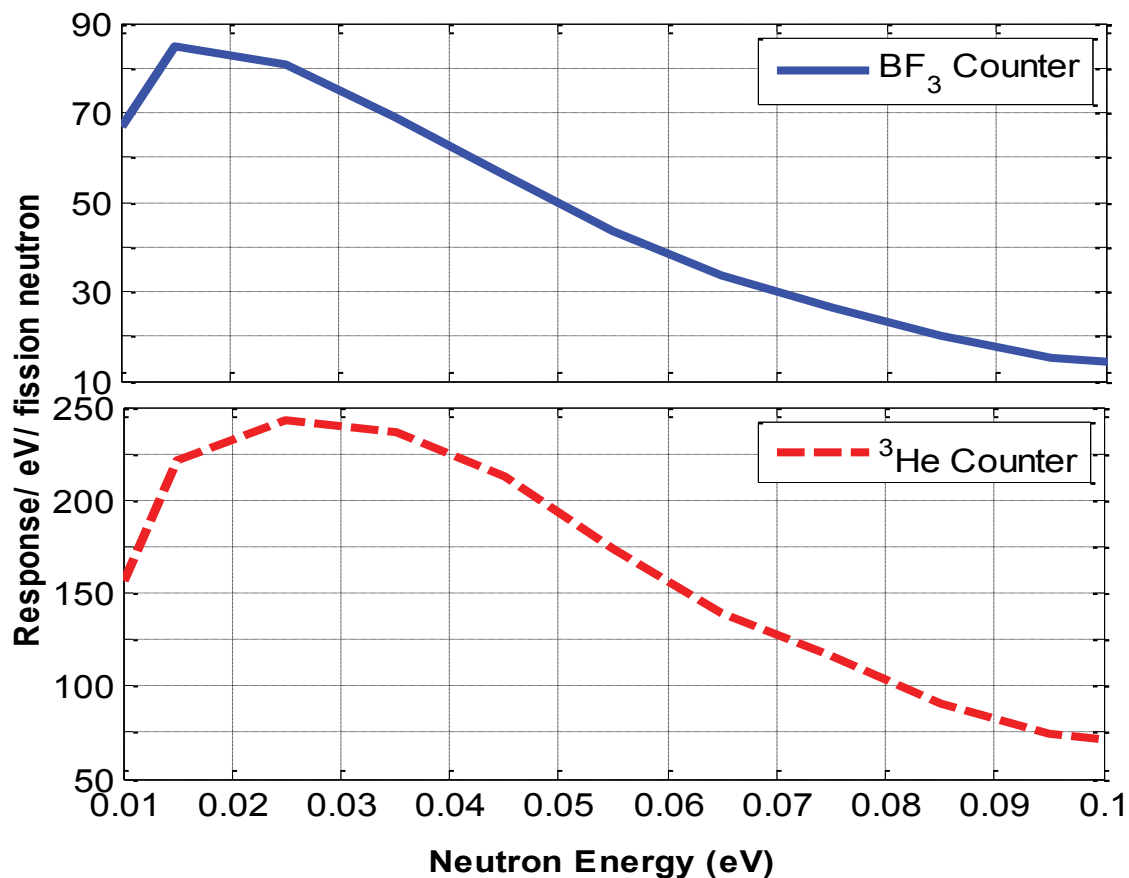
Figure 3: Responses for BF$_3$ and ^{3}He counters to thermal neutrons

chamber. This results in a current flow between the electrodes. The current is subsequently detected and converted into voltage pulses, which are translated into neutron flux measurements [14]. Thus, a second approach that involves tracking the charged-particle energy depositions (pulse height distributions) inside the two detectors has been used in this study. For the case of BF$_3$ counter, the simulation was able to track energy depositions for alpha particles and lithium ions, whereas for the ^{3}He counter, energy depositions for the generated protons and triton were tracked and their pulses tallied [7].

Typical BF$_3$ pulse height distribution

When thermal neutron is absorbed by ^{10}B component of the detector's fill-gas, ^{10}B (n,α) ^{7}Li reaction occurs and the emitted alpha particle and recoil ^{7}Li nucleus travel off in opposite directions in order to conserve the momentum [12]. It's well described in literature [12,14], that a typical result of the reaction falls into two categories: 1) reaction product ^{7}Li is left in a ground, 2) reaction product ^{7}Li is left in an excited state. When the lithium nucleus is left in the excited state (which is about 94% of the time), it quickly returns (i.e., half-life of ~10^{-13} s) to the ground state, emitting 0.84 MeV γ-rays plus a useful *Q*-value of 2.31 MeV which is shared by the alpha (1.47 MeV) and ^{7}Li (0.84 MeV) nuclei [14]. Alpha particle takes a larger portion of the energy because it's lighter than ^{7}Li nucleus [12].

When the ^{7}Li is left in the ground state (about 6% of the time), the alpha and lithium nuclei share a much larger full *Q*-value of 2.79 MeV since there is no gamma emission in this case. In both cases, the *Q*-value of the reaction is very large (2.31 or 2.79 MeV) compared with the incoming energy of the slow neutron, so that the energy imparted to the reaction products is essentially just the *Q*-value itself [14]. Figure 4 shows the pulse height distribution for a 2.438 cm wide and 31.12 cm long BF$_3$ counter filled at a pressure of 0.3 atm. It can be seen from Figure 4 that the pulse height spectrum has more than two peaks - a large one at about 2.31 MeV, a small one at about 2.79 MeV and several edges to the left of the 2.31 MeV peak. For this typical case, the full peak at excited registered about 8.0 × 10^{-5} pulses/MeV/ particle while the full peak at ground state registered only about 0.3 × 10^{-5} pulses/MeV/particle.

Like in any other gas-filled detector, the pulse height spectra of a BF$_3$ counter strongly depends on the distance traveled by the reaction products (alpha and ^{7}Li) and where they deposit their kinetic energies following their formation. When

all the kinetic energies of the alpha particle and recoil ^{7}Li nucleus are deposited in the detector fill-gas, a pulse height spectrum with only two peaks is expected. These are the peaks at 2.31 MeV (for excited state) and 2.79 MeV (for ground state) observed in Figure 4. The smaller pulses observed on the left of the 2.31 MeV peak in Figure 4 occurred because either the alpha particle or ^{7}Li nucleus deposits some of its energy in the detector wall rather than the gas. This phenomenon is predominantly observed in gas-filled detectors and it's commonly referred to as the *wall-effect* [14].

The wall-effect is a clear indication that not all the charged particles produced will contribute to the useful output signal of the detector. Only rarely would the alpha particle and ^{7}Li nucleus both strike the detector wall because they are emitted in opposite directions. When the neutron interaction takes place in the gas close enough to one side of the tube for either the alpha particle or lithium nucleus to strike the wall, the distance to the other side of the tube would be greater than the range of the particle heading towards it. The resulting wall effect normally creates two steps on the left side of the 2.31 MeV peak. The first edge to the far left observed in Figure 4 is produced as a result of the alpha particle striking the wall and the ^{7}Li depositing all its energy (0.84 MeV) in the gas. The second edge which resulted from the ^{7}Li nucleus striking the wall and the alpha particle depositing all its energy (1.47 MeV) in the gas cannot be clearly observed in Figure 4. The rest of the peaks observed in Figure 4 are the wall-effect continuum which extends from E_{Li} (0.84 MeV) up to the full-energy peak at ($E_{Li}+E_a$) (2.31 MeV).

Typical ^{3}He pulse height distribution

When ^{3}He gas absorbs thermal neutron, it undergoes ^{3}He (n,p) ^{3}H reaction liberating 0.764 MeV of energy as the reaction *Q*-value. The *Q*-value is shared by the oppositely directed reaction products; proton and triton, with proton carrying a larger amount (0.573 MeV) than triton (0.191 MeV) [1]. Figure 5 shows the pulse height spectrum for ^{3}He counter simulated with fill-gas pressure of 3 atm.

Like for the case of BF$_3$, the response function of this detector also depends on the distance traveled by the reaction products (proton and triton) and where they deposit their kinetic energies following their formation. When all the
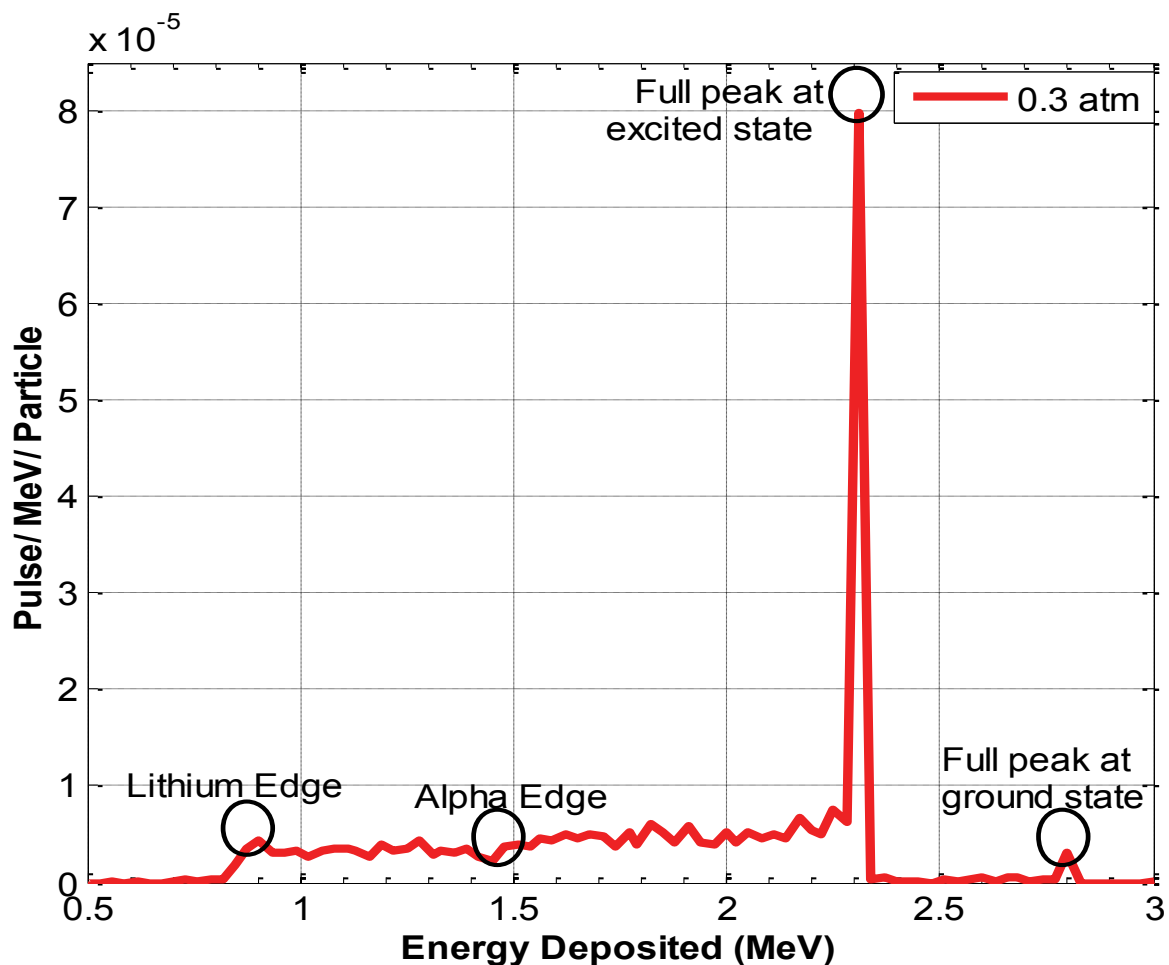

Figure 4: Pulse height spectrum for BF$_3$ counter at 0.3 atm
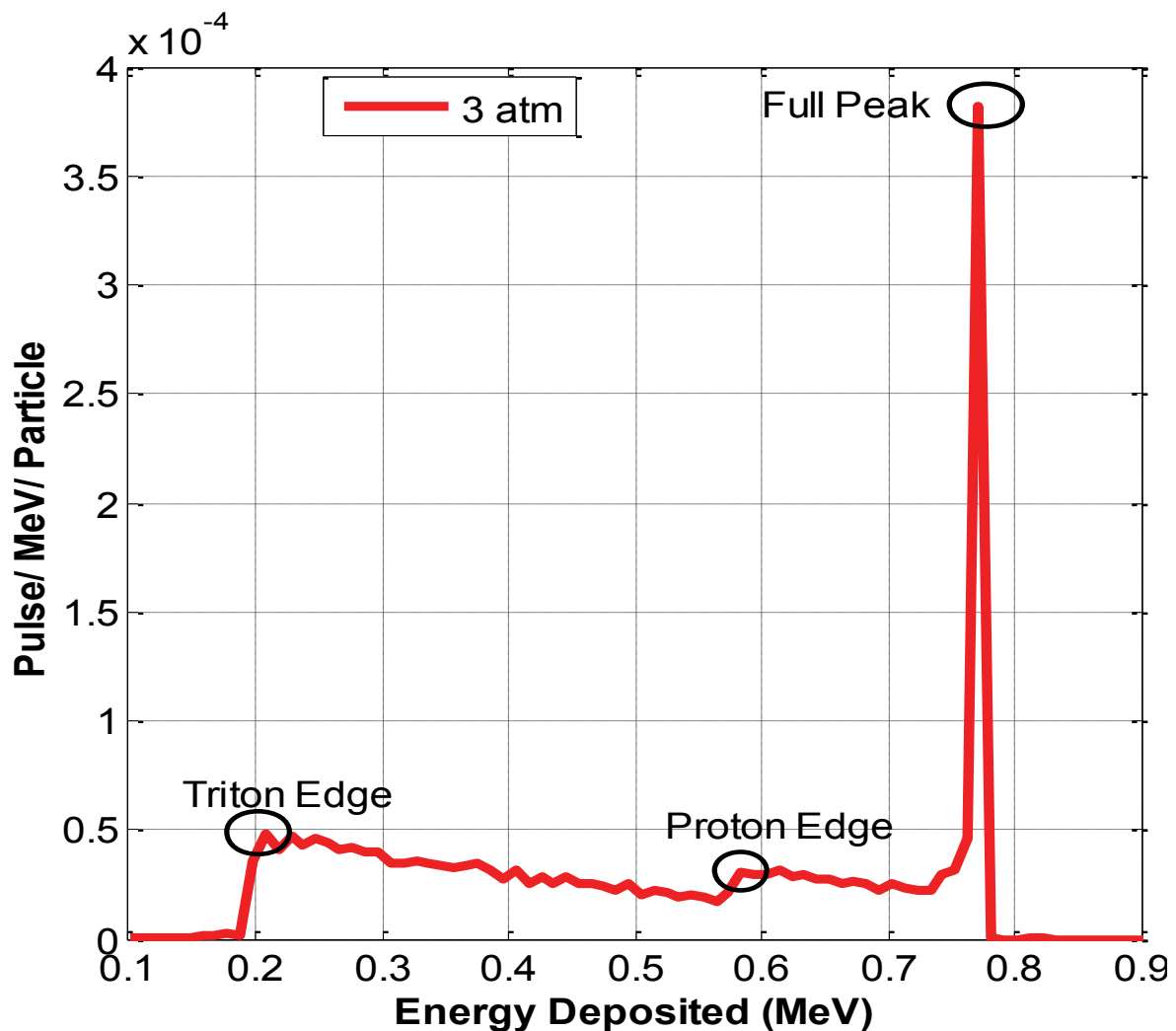
Figure 5: Pulse height spectrum for a [3]He counter at 3 atm

kinetic energies of proton and triton are deposited in the detector fill-gas, a pulse height spectrum with only one peak is expected at 0.764 MeV as seen in Figure 5. The greater the energy deposited in the gas by these particles, the larger the number of primary ion pairs, the larger the number of avalanches and the larger the pulse detected as the output signal by the electronic acquisition chain. For the case of this study, it can be seen from Figure 5 that the full peak registered about 3.8×10^{-4} pulses/MeV/particle.

Like any other gas-filled detector, [3]He counters also suffer from the wall-effect phenomenon explained earlier [10]. This accounts for the smaller pulses observed on the left of the 0.764 MeV peak in Figure 5 When the [3]He (n,p) ^{3}H reaction takes place close to detector walls, it is possible for proton to go toward the wall effectively without depositing its energy in the gas [1]. However, because proton and triton are emitted in opposite directions, such events correspond to triton moving away from the wall into the bulk gas. Thus, the minimum energy deposited in the counter is 0.191 MeV, which is the kinetic energy of triton. Triton edge is the first characteristic feature that appears in the pulse height spectrum of Figure 5.

In the opposite case, when triton strikes the cathode wall without depositing energy in the gas, proton heading in the opposite direction can deposit 0.574 MeV. This explains the second prominent edge characteristic in the spectrum, also called *proton edge* [1,7]. Between these two extremes, the energy deposited in the gas includes a fraction of either the proton or triton edges. This is called the *wall-effect continuum*. Perhaps, the most important point to note is that there is no information about the primary neutron spectrum. All of the events of interest fall into one peak, which is the reaction energy (0.76 MeV).

Effect of tube pressure on response functions

The effects of increasing tube pressure on response functions of BF$_3$ and [3]He counters were also investigated in this

study. Detailed investigations included simulating the effects of pressure on the number of ^{10}B (n,α) ^7Li and ^3He (n,p) ^3H absorption reactions inside BF_3 and ^3He counters respectively. Also investigated were the effects of increasing tube pressure on the pulse height distributions. Pressure for the BF_3 tube was varied between 0.1 and 1.4 atmospheres, while that of ^3He tube was varied between 1 and 14 atmospheres. ^3He gas-filled counter was operated at higher pressures because ^3He gas itself is a much lighter gas compared to BF_3 gas. At low pressure, ^3He is found not sufficiently dense enough to stop all the proton and triton particles emerging from the detection reaction [15].

Figure 6 is the normalized simulated number of ^{10}B (n,α) ^7Li and ^3He (n,p) ^3H reactions versus tube pressure. Generally, it can be seen from Figure 6 that both counters' responses increased with increasing pressure. For the case of BF_3 counter, the response was near-linear, whereas for ^3He counter it was an exponential increase. According to Desai and Shaik [15], ^3He gas is not sufficiently dense enough to stop all the charged particles generated even at high pressures. That means increasing pressure in ^3He tube only slightly increases the chances for ^3He (n,p) ^3H reaction. For most commercially available ^3He counters, tube pressure is limited to about 4-8 atm [7].

BF_3 pulse height

Figure 7 shows the effects of increasing tube pressure on pulse height spectra for BF_3 counter. The simulation was performed for four different tubes at fill-gas pressures of 0.3, 0.5, 1.0 and 1.4 atm. Generally, it can be seen from Figure 7 that increasing fill-gas pressure made two significant improvements to the tube performance; 1) increased the pulse height spectra, and 2) reduced the wall-effect phenomena.

For instance when the tube pressure was 0.3 atm, significantly large continuums of peaks resulting from the wall-effect phenomena were observed to the left of the full peak, and the full peak at excited state registered approximately 0.8×10^{-4} pulses/MeV/particle. When the tube pressure was increased from 0.3 atm to 1.4 atm through 0.5 atm and 1.0 atm, significant reduction in the wall-effect phenomena was observed as the continuum peaks diminished with increasing pressure. Also the pulse height increased from 0.8×10^{-4} pulses/MeV/particle at 0.3 atm to 8.6×10^{-4} pulses/MeV/particle at 1.4 atm (Figure 7).
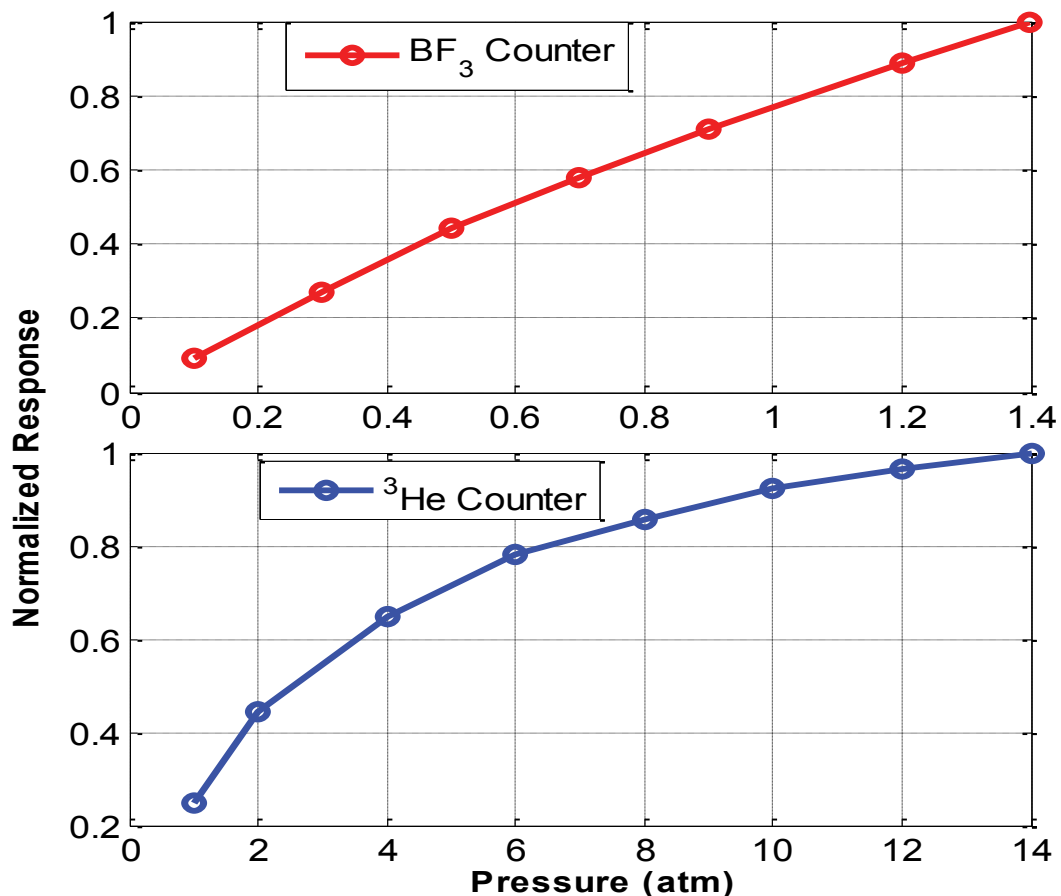

Figure 6: Effect of pressure on the response functions of BF_3 and ^3He counters
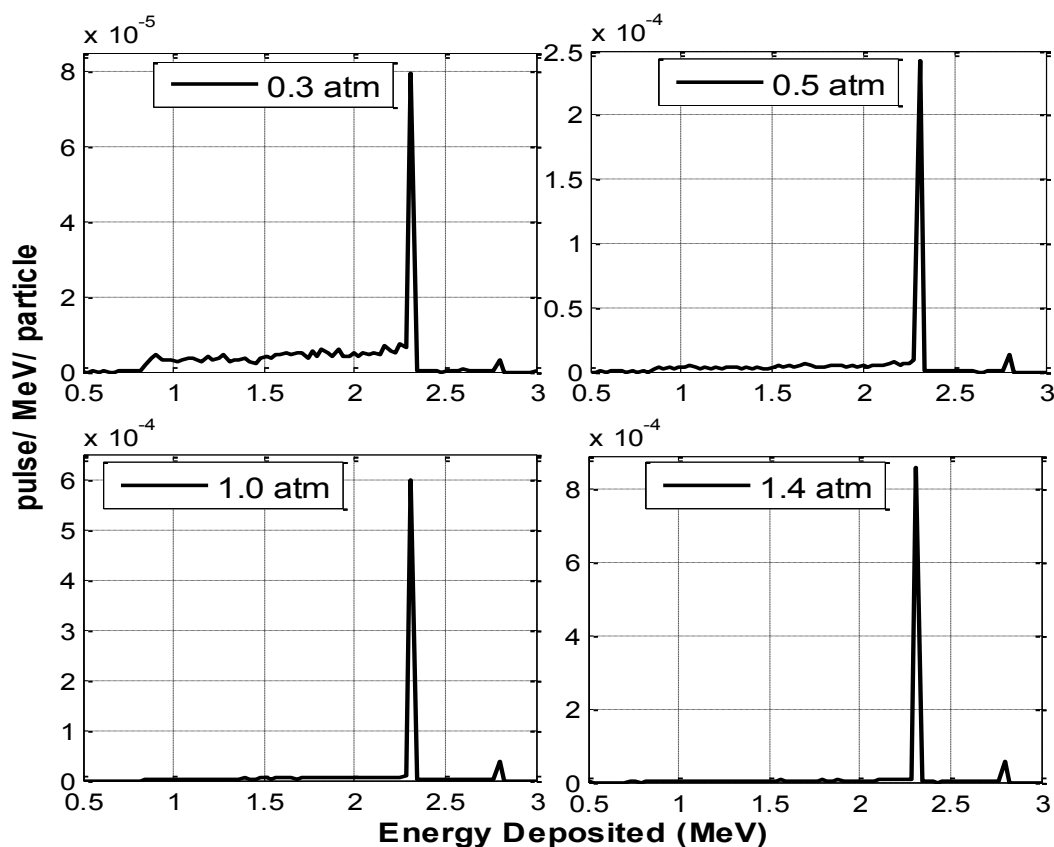
Figure 7: Effect of pressure on pulse height distribution of a BF_3 counter

The wall-effect phenomenon observed in BF_3 is caused by boron reactions which occur on or close to the walls of the counter. According to Andersson and Malmskog [16], when the ^{10}B (n,α) ^7Li reaction takes place near the walls of the counter, one of the reaction fragments is likely to reach the wall without all its energy being dissipated into ionization in the gas. This so called wall-effect gives rise to the continuous distribution on the low energy sides of the peaks in the pulse height spectrum [1,7]. The wall-effect is directly related to the range of the reaction fragments, and can thus be lowered by increasing the gas pressure in the counter [16]. Also, the observed increase in pulse heights with increasing tube pressures implies the enormous fill-gas molecules in the tube are able to absorb most of the emitted alpha and lithium (Figure 7).

Much as increasing tube pressure helps to enhance the detector performance by reducing the wall-effect phenomena and increasing pulse heights, studies have shown there is a pervading tendency that the energy resolution of the detector deteriorates when operated at very high pressures beyond 2 atm [12,14,16,17]. The reason for this may be that there are impurities in the gas that have not been removed by the purification process or that the boron trifluoride has a certain electron affinity.

^3He pulse height

Figure 8 shows the pulse height spectra for ^3He counter simulated at pressures of 1.0, 3.0, 5.0 and 10 atm. Like in the case of BF_3 counter, increasing ^3He tube pressure was observed to help reduce the wall-effect phenomenon as well as cause increase in the pulse heights. However, here the counter must be operated at higher pressures than for BF_3 counter because ^3He gas is light. When the counter was simulated at 1.0 atm, the expected total full energy peak at 0.76 MeV is so small (only ~0.15×10^{-4} pulses/MeV/particle) compared to the triton edge (observed at around 0.2 MeV) which recorded ~0.82×10^{-4} pulses/MeV/particle. This shows that at 1.0 atm, ^3He fill-gas is not dense enough to stop most of the protons. The maximum energy recorded here is therefore the kinetic energy of triton (Figure 8).

When the counter was operated at 3.0 atm, proton escape was significantly reduced and the total full energy peak at 0.76 MeV rose up, registering significant counts (~3.80×10^{-4} pulses/MeV/particle). On the left of this peak were large triton edge, proton edge and the wall-effect continuums. At 5.0 atm, the wall-effect was further minimized. When the tube was simulated at 10 atm, the wall-effect was observed to be very small. Pulse heights were also seen to increase
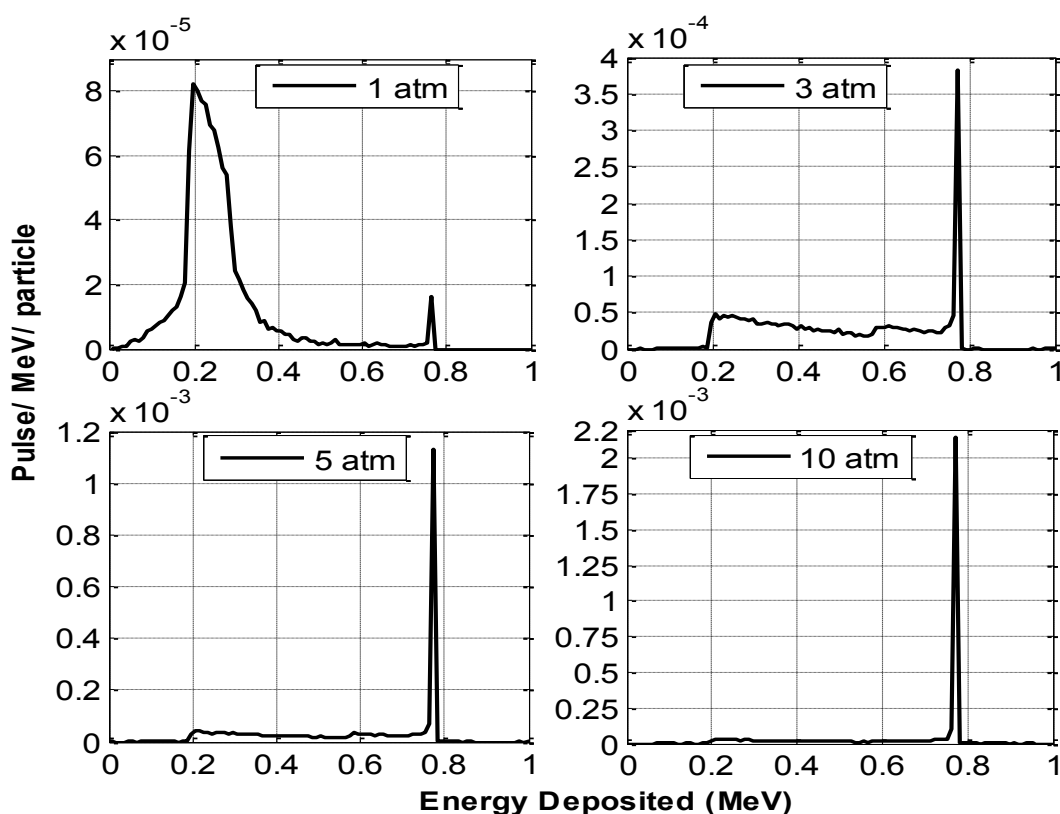
Figure 8: Effect of pressure increase on pulse height distribution of a ³He counter

to ~1.13 × 10⁻³ pulses/MeV/particle at 5 atm and ~2.13 × 10⁻³ pulses/MeV/particle at 10 atm. Thus, increasing ³He tube pressure was observed to cause an overall increase in efficiency of both counters.

Effect of increasing tube diameter on response functions

Also investigated in this study were the effects of increasing tube diameter on the response functions of BF₃ and ³He counters. This involved simulating the numbers of absorption reactions, as well as the resultant pulse height distributions in the two counters. The tube diameters used in this simulation (for both BF₃ and ³He counters) were 1, 2.5, 4 and 6 cm. Figure 9 presents the normalized number of absorption reactions inside BF₃ and ³He counters versus tube diameters. It should be noted that in this case, pressure inside the counters were kept constant at 1 atm and 10 atm for the BF₃ and ³He counters, respectively.

As seen from Figure 9, the response functions for both BF₃ and ³He counters increased with increasing tube diameter. For the case of BF₃ counter, the response was near-linear, whereas for ³He counter it was an exponential increase. This implies that increasing diameter for ³He counter's tube only slightly increases the chances for ³He (n,p) ³H reaction.

BF₃ pulse height

Figure 10 shows typical pulse height spectra of a BF₃ counter with diameters of 1.0, 2.5, 4.0 and 6 cm. In this particular case the tubes were maintained at constant pressure of 1 atm. Generally, it can be observed from Figure 10 that increasing the BF₃ tube diameter caused significant increase in the detector's pulse heights. When the tube diameter was 1 cm, the full peak at excited state registered only about 7.5 × 10⁻⁵ pulse/MeV/particle compared to ~6.3 × 10⁻⁴ pulse/MeV/particle registered when the tube diameter was increased to 2.5 cm. When the tube diameter was further increased to 4 cm, there was an observed further increase in the detector's pulse height to approximately 1.46 × 10⁻³ pulse/MeV/particle. However, increasing tube diameter beyond 4 cm registered no more increase in the detector's pulse height. This was evident when a 6 cm wide tube registered the same pulse (i.e., ~1.46 × 10⁻³ pulse/MeV/particle) as a 4 cm tube as seen in Figure 10. This implies that the 4 cm wide counter was large enough to collect nearly all the alpha particles and lithium nuclei generated when ¹⁰B absorbs thermal neutrons.

Also observed from Figure 10 was that increasing tube diameter helped to significantly reduce the wall-effect phenomena. With tube diameter of 1 cm, large wall-effect continuums were observed to the left of the tallest peak. The
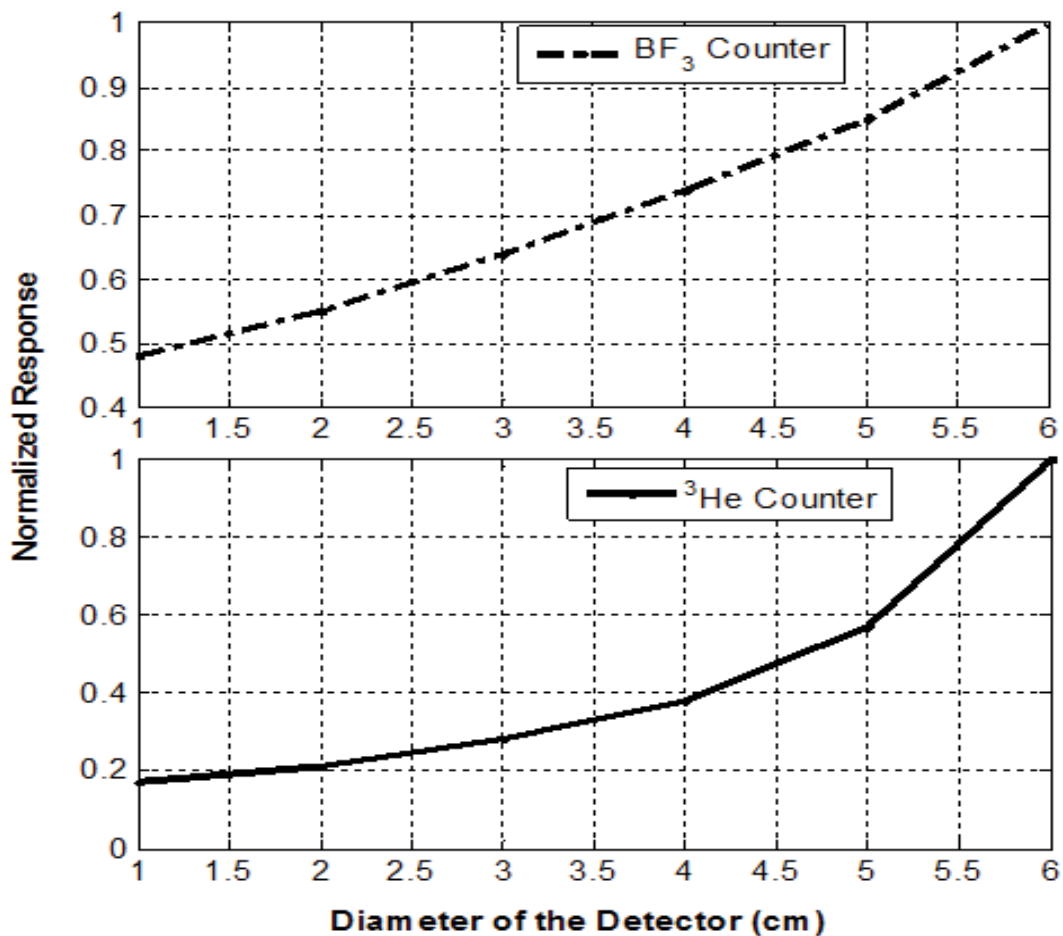
Figure 9: Effect of increasing tube diameter on the response functions

wall-effect occurred because the tube was not large enough to stop all the alpha particles and lithium nuclei to deposit all their kinetic energies within the fill-gas. Thus, some of the alphas and lithium nuclei emitted close to the detector walls were able to deposit part of their kinetic energies in the fill-gas before being absorbed at the walls. However, when the tube diameter was increased to 2.5 cm, there was a significant reduction in the wall-effect phenomenon, implying most of the alphas and lithium nuclei were stopped within the fill-gas. At 4 cm and beyond, there was almost no wall-effect phenomenon observed.

He pulse height

Figure 11 shows the effect of increasing tube diameter on ^{3}He pulse height spectra. Like for the case of BF_3 counter, increasing ^{3}He tube diameter was observed to cause significant increase in the detector's pulse heights. With tube diameter of 1 cm, the full energy peak recorded $\sim 4.3 \times 10^{-4}$ pulse/MeV/particle. While for the 2.5 cm wide tube, the pulse height increased to $\sim 2.3 \times 10^{-3}$ pulse/MeV/particle. For the 4 and 6 cm wide tubes, there was a uniform response of $\sim 3.8 \times 10^{-3}$ pulse/MeV/particle. No increase in pulses was observed when the tube diameter was increased beyond 4 cm because most of the triton and protons will have been absorbed in the fill-gas.

Also observed from Figure 11 was the significant reduction of wall-effect phenomenon. Just like explained earlier for the case of BF_3 counter, with counter diameter of 1 cm, large wall-effect continuums were observed. This occurred because the tube was not large enough to stop all the emitted triton and protons to deposit their kinetic energies within the fill-gas. Thus, some of the triton and protons were able to deposit part of their kinetic energies in the fill-gas before being absorbed at the walls. When the tube diameter was further increased to 2.5 cm, there was a significant reduction in the wall-effect phenomenon, implying most of the triton and protons were stopped within the fill-gas. At 4 cm and beyond, there was almost no wall-effect phenomenon observed.
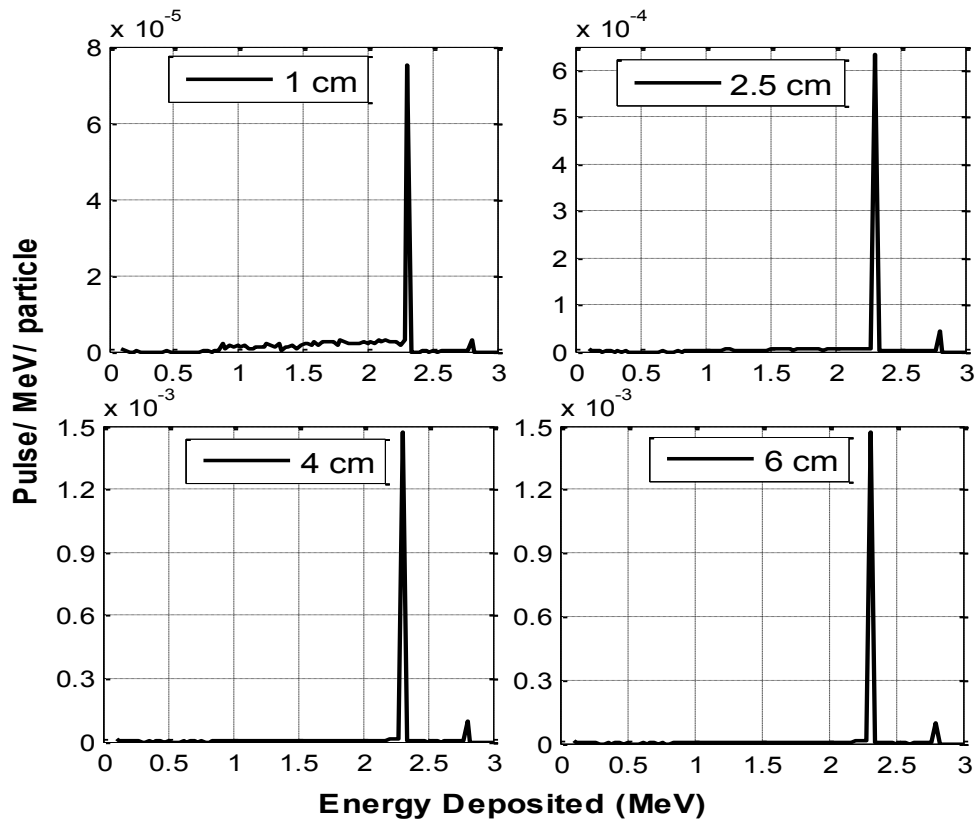
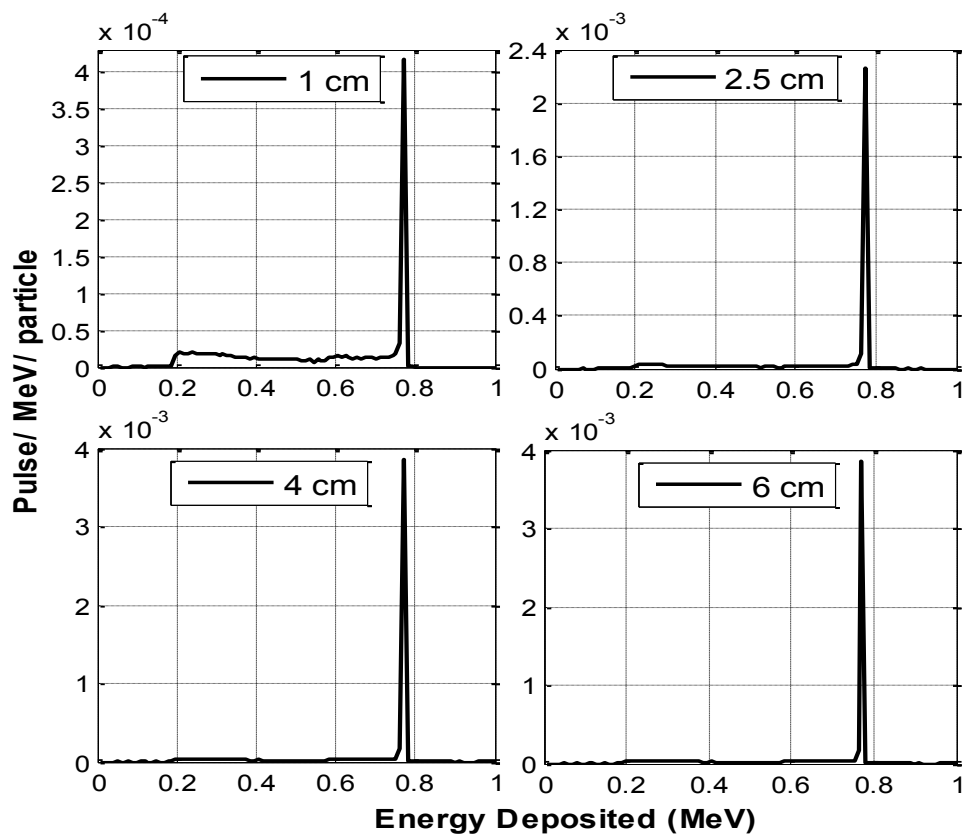**Figure 10:** Effect of increasing tube diameter on BF$_3$ counter's pulse height spectra

Figure 11: Effect of increasing tube diameter on pulse height spectra of ^{3}He counter

CONCLUSION

The response functions of ^{3}He and BF$_3$ counters to thermal neutrons at OPAL reactor were simulated in this study using MCNPX code. The study showed that material composition of the reactor core affects thermal neutron flux distribution. High flux was observed at the center of the reactor core. Thermal flux decayed with increasing radial distance from the core center. Generally, the number of absorption reactions in the two counters decreased gradually with increasing neutron energy. ^{3}He counter registered higher responses than the BF$_3$ counter. Pulse height spectra with two peaks were observed in BF$_3$ counter when all the kinetic energies of the emitted alpha particles and recoil ^{7}Li nuclei were deposited in the detector's fill-gas. The tallest peak was observed at 2.31 MeV (for excited state) and a short one at 2.79 MeV (for ground state). For the case of ^{3}He counter, a pulse height spectrum with a single peak was observed at 0.76 MeV. This occurred when all the liberated triton and proton lose their kinetic energies inside the detector's fill-gas.

The number of absorption reactions inside the two counters was seen to increase with increasing tube pressure and tube diameter. Also, increases in tube pressure and tube diameter were observed to have caused reasonable increase in the pulse heights for both counters. However, for tubes with diameter larger than 4 cm, there were no observed increases in pulse heights for both counters. Also, increasing tube diameter and tube pressure helped to reduce the wall-effect phenomenon, which is common in gas-filled detectors.

ACKNOWLEDGEMENT

REFERENCES

[1] Takeda N, Kudo K. Neutron response functions improved by taking into consideration measured edge effect of ^{3}He proportional counter. *IEEE Trans Nucl Sci*, **1994**, 41: 880e883.

[2] Samir AMA. New neutron detector using magnetically focused electrons for fast reactor neutron flux measurements. PhD Thesis, Georgia Institute of Technology, Georgia, **1976**.

[3] Knoll GF. Radiation detection and measurement. John Wiley and Sons Inc., USA, **2000**.

[4] Hashemi-Tilehnoee M, Javidkia F. Improving the performance of the power monitoring channel. *Nuclear Reactors*, InTech, **2000**.

[5] Gallardo S, Rodenas J, Verdu G. Monte carlo simulation of the Compton scattering technique applied to characterize diagnostic x-ray spectra. *Med Phys*, **2004**.

[6] Pelowitz DB. MCNPX User's Manual Version 2.7.0, **2011**.

[7] Mazed D, Mameri S, Ciolini R. Design parameters and technology optimization of ^{3}He-filled proportional counters for thermal neutron detection and spectrometry applications. *Radiat Meas*, **2012,** 47: 577-587.

[8] Schillebeeckx P. Characterization of ^{3}He proportional counters. *Radiat Meas*, **2006**, 41: 582-593.

[9] Harvey, Zachary R. Neutron flux and energy characterization of a plutonium-beryllium isotopic neutron source by Monte Carlo simulation with verification by neutron activation analysis. UNLV Theses/Dissertations/Professional Papers/Capstones, **2010.**

[10] Beddingfield DH, Johnson NH, Menlove HO. ^{3}He neutron proportional counter performance in high gamma-ray dose environments. Nucl Instr Meth A, **2000**, 455: 670e682.

[11] Summerfield MW. Licensing of the OPAL reactor during construction and commissioning. IAEA CN-156/S-37/ OR, **2007**.

[12] Andersson J. Simulation of neutron fluxes around the W7-X stellarator. Royal Institute of Technology, Stockholm, Sweden, **1999**.

[13] Amgarou K, Lacoste V. Response matrix evaluations of a passive Bonner sphere system used for neutron spectrometry at pulsed, intense and complex mixed fields. IOP Publishing Ltd. and SISSA, **2010.**

[14] Nasimi E, Gabbar H. Analysis of operational challenges of existing start-up instrumentation for CANDU reactors at Bruce power Stations. Presentation at an International Workshop on Real Time Measurement, Instrumentation and Control, IEEE NPSS, Oshawa, **2010**.

[15] Desai SS, Shaik AM. On studies of ^{3}He and isobutane mixture as neutron proportional counter gas. *Nucl Instr Meth A,* **2006**, 557: 607-614.

[16] Andersson O, S Malmskog. Investigation of the pulse height distribution of boron trifluoride proportional counters. Aktiebolaget Atomenergi, **1962**.

[17] Yamane M. A study of pulse height distribution of boron trifluoride proportional counters. *Phys Soc Japan*, **1960**, 15: 1732.